High-Resolution Metabolite Imaging of Light and Dark Treated Retina Using MALDI-FTICR Mass Spectrometry

Na Sun[1]‡, Alice Ly[2]‡, Stephan Meding[1,3], Michael Witting[4], Stefanie M. Hauck[2], Marius Ueffing[2,5], Philippe Schmitt-Kopplin[4], Michaela Aichler[1], Axel Walch[1].*

[1]Research Unit Analytical Pathology, Institute of Pathology, Helmholtz Zentrum München, German Research Center for Environmental Health (GmbH), Neuherberg, Germany.

[2]Research Unit Protein Science, Helmholtz Zentrum München, German Research Center for Environmental Health (GmbH), Neuherberg Germany.

[3]Adelaide Proteomics Centre, School of Molecular and Biomedical Science, The University of Adelaide, Adelaide, Australia

[4]Department of Environmental Sciences, Research Unit Analytical BioGeoChemistry, Helmholtz Zentrum München, German Research Center for Environmental Health (GmbH), Neuherberg Germany.

[5]Center of Ophthalmology, Institute for Ophthalmic Research, University of Tübingen, Tübingen, Germany.

Received: September 16, 2013; Revised: December 06, 2013; Accepted: December 20, 2013

This article has been accepted for publication and undergone full peer review but has not been through the copyediting, typesetting, pagination and proofreading process, which may lead to differences between this version and the Version of Record. Please cite this article as doi: 10.1002/pmic.201300407.

Corresponding Author

*Axel Walch

Research Unit Analytical Pathology, Institute of Pathology

Helmholtz Zentrum München, German Research Center for Environmental Health (GmbH), Neuherberg, Germany.

E-mail: axel.walch@helmholtz-muenchen.de

Phone: +49-89-3187-2739

Fax: +49-89-3187-3349

Author Contributions

The manuscript was written through contributions of all authors. All authors have given approval to the final version of the manuscript.

‡These authors contributed equally.

KEYWORDS

- FTICR
- MALDI
- Mass spectrometry imaging

- Metabolomics
- Retina

Abstract Word Count – 166

Total Text Word Count – 6574

ABBREVIATIONS

9-AA, 9-aminoacridine; ACN, acetonitrile; DR, diabetic retinopathy; F1,6bP, fructose-1,6-bisphosphate; G6P, glucose-6-phosphate; G6PD, G6P dehydrogenase; HE, haematoxylin and eosin; MALDI-FTICR, Matrix-assisted laser desorption/ionization-Fourier transform ion cyclotron resonance; MSI, mass spectrometry imaging; NAA, *N*-acetylaspartate; TCA, tricarboxylic acid

ABSTRACT

Mass spectrometry imaging (MSI) is a valuable tool for diagnostics and systems biology studies, being a highly sensitive, label-free technique capable of providing comprehensive spatial distribution of different classes of biomolecules. The application of MSI to the study of endogenous compounds has received considerable attention because metabolites are the result of the interactions of a biosystem with its environment. MSI can therefore enhance understanding of disease mechanisms and elucidate mechanisms for biological variation. Here we present the *in situ* comparative metabolomics imaging data for analyses of light- and dark-treated retina. A wide variety of tissue metabolites were imaged at a high spatial resolution. These include nucleotides, central carbon metabolism pathway intermediates, 2-oxocarboxylic acid metabolism, oxidative phosphorylation, glycerophospholipid metabolism,

and cysteine and methionine metabolites. The high lateral resolution enabled the differentiation of retinal layers, allowing determination of the spatial distributions of different endogenous compounds. A number of metabolites demonstrated differences between light and dark conditions. These findings add to the understanding of metabolic activity in the retina.

1. INTRODUCTION

Metabolomics is emerging as an increasingly important systems biology tool which can provide information on the metabolic phenotype of a cell, tissue or organism during normal and pathological conditions. Because metabolic phenotypes are not only affected by gene expression and protein function but also by environmental factors [1, 2], metabolomics has been described as the link between the genotype and the phenotype [1]. Mass spectrometry is currently the favored method for metabolomics studies due to its ability for the direct and simultaneous analysis of many compounds [2, 3]. One drawback, however, is that sample processing steps can result in the loss of spatial information inherent in the tissue. Mass spectrometry imaging (MSI) is a rapidly evolving technology which enables the visualization of many substances within a single sample, and allows for the virtual dissection of tissue based on molecular mass signatures [4-6]. Matrix-assisted laser desorption/ionization-Fourier transform ion cyclotron resonance (MALDI-FTICR) instruments provide the highest resolving power and mass accuracy, and have been used for the imaging of peptides, drugs and drug metabolites [7-9]. Although these instruments have a relatively low through-put, the advantages of combining MALDI-FTICR-MS with MSI is that, compared to traditional mass spectrometry or immunohistochemistry, this combined technique is able to simultaneously detect and spatially localize many compounds within cells and tissues without the use of labeling. This is especially important for substances with a low molecular weight or those

which are difficult to resolve with imaging techniques, for example downstream metabolic products of glucose metabolism.

The retina is the extension of the central nervous system where light is converted into sensory information. A consequence of this specialized function is that retinal metabolic demands differ depending on dark or light conditions and cell class [10, 11]. The retina has a distinctive anatomy consisting of alternating layers of neurons and synapses (see figure 3). Light-converting photoreceptor outer segments are located in the posterior (distal) outer retina, while the mitochondria-heavy photoreceptor somata are located in the outer nuclear layer of the anterior outer retina. Photoreceptors synapse with signal-converting bipolar cells of the inner retina, which subsequently form synapses with ganglion cells whose axons project to the brain [12]. Consumption of oxygen and glucose are much higher in the photoreceptor-heavy outer retina in the dark than in light [10, 13], which is largely due to neurotransmitter release and Na^+/K^+-ATPase activity [14-16]. In contrast, glucose metabolism and oxygen consumption within the inner retina has been reported to stay largely constant, independent of light or dark exposure [11, 17]. Defects in retinal metabolism can lead to visual dysfunction, as seen in Leber's hereditary optic neuropathy where mitochondrial function is compromised [18], and in the systemic metabolic disorder diabetes [19, 20], while accumulation of free radicals has been linked to oxidative stress in age-related macular degeneration [21]. As such, a greater understanding of retinal metabolism and metabolites would enhance our understanding of retinal physiology, and how it is altered under different conditions.

In this study, we performed *in situ* metabolomic imaging of light- and dark-treated retina using MALDI-FTICR-MSI. A wide variety of tissue metabolites were imaged with high

spatial resolution. The high lateral resolution enabled separation of retinal layers and resolved the spatial distribution of different endogenous biocompounds. In particular, the distribution of metabolites associated with glycolysis and the tricarboxylic acid (TCA) cycle of the central carbon metabolism pathway are significantly altered under light and dark conditions. These findings add to the understanding of retinal physiology.

2. MATERIALS AND METHODS

2.1 Preparation of porcine retina samples

Adult porcine eyes (5 biological replicates per condition) were acquired from a local slaughterhouse. To create our experimental groups, the eyes were either maintained in the dark or exposed to direct light post-mortem. Samples allocated as 'dark-treated' were immediately stored in the dark following collection, and dissected and sectioned using dim red LED illumination, which produces minimal impact on photopigment activation [22]. Light-treated eyes were illuminated from a desk lamp at 1850 lux for 30 minutes. To minimize heat-induced artifacts, these eyes were immersed in tris-buffered saline (TBS) and received the light-treatment from a distance of 30 cm. Light-treated eyes were then processed under normal laboratory lighting. The cornea, lens, and vitreous humor were removed, and the posterior chamber (retina and sclera) were immediately frozen in liquid nitrogen. The eyes were frozen onto the chuck using water, and peripheral retina transversely cryosectioned at 12 μm (CM1950, Leica Microsystems, Wetzlar, Germany) using a fine brush on the sclera to guide the section from the blade. Sections were thaw mounted onto indium-tin-oxide-coated conductive slides (Bruker Daltonik, Bremen, Germany).

The sections were coated with 9-aminoacridine (9-AA) hydrochloride monohydrate matrix (Sigma-Aldrich, Germany) at 10 mg/ml in water/methanol 30:70 (v/v) by a SunCollect^{TM} automatic sprayer (Sunchrom, Friedrichsdorf, Germany). Fine droplets of matrix were

deposited onto the tissue section at variable flow rates over 8 layers. The first three layers were performed at 10 µl/min, 20 µl/min and 30 µl/min, respectively. The last five layers were set at 40 µl/min.

2.2 MALDI mass spectrometry imaging

MSI was performed using a Bruker Solarix 7T FTICR-MS (Bruker Daltonik, Bremen, Germany) in negative ion mode. Ions were detected over a mass range of *m/z* 50 to 1000 with a lateral resolution of 50 µm. For identification of metabolites, MS/MS analysis was conducted using continuous accumulation of selected ions mode, which allows the target ions to be selected in the quadrupole and accumulated in the collision cell. Metabolites were either identified by comparing the observed MS/MS spectra with standard compounds or by matching accurate mass with databases (METLIN, http://metlin.scripps.edu/; MassBank, http://www.massbank.jp/; and Human Metabolome Database, http://www.hmdb.ca/).

MSI images were generated using FlexImaging v. 4.0 software (Bruker Daltonik). MALDI ionization has been known to cause both spot-to-spot and sample-to-sample variations in signal intensities due to the heterogeneity of matrix crystals. To remove variations in pixel-to-pixel intensity, the signal for each pixel was normalized against the root mean square of all data points using FlexImaging v. 4.0 software. This normalization process is critical for quantitative comparison of MSI data acquired from different tissue sections.

2.3 Haematoxylin and Eosin Staining

Following MSI measurement, the matrix was removed with 70% ethanol, and the sections stained with haematoxylin and eosin (HE), coverslipped, and scanned using a 20x

magnification objective on a Mirax Desk slide scanner (Carl Zeiss MicroImaging, Göttingen, Germany). The scans were co-registered with the MSI data to correlate the mass spectrometry data with the histological features of the corresponding region.

2.4 Metabolite extraction and LC-(MS/MS)

80 mg of porcine retina tissue was placed in NucleoSpin BeadTube (Macherey Nagel, Düren, Germany) with 1 ml of cold 80% MeOH/20% water. The tissue was lysed for 3 minutes at a frequency of 30 Hz using a TissueLyser (Qiagen, Hilden, Germany), centrifuged at 17,900 g at 4°C for 15 minutes and transferred to an autosampler vial.

LC-MS(/MS) was used to confirm the identities of various retinal metabolites against standards (Sigma-Aldrich, Munich, Germany; see Table 1) on a XBridge Amide column, 100 mm x 4.6 mm ID, 3.5 µm (Waters, Eschborn, Germany) using an established protocol [23]. Briefly, 10 µl of retina sample and 10µg/ml of single metabolite standards were injected on the column via full loop injection. Separation was carried out on a Waters Acquity UPLC (Waters, Eschborn, Germany) coupled to maXis UHR-TOF-MS (Bruker Daltonics, Bremen, Germany), at a flow rate of 300 µl/min, using the same gradient conditions as Yuan et al. [23]. Buffer A consisted of 20 mM ammonium hydroxide and 20 mM ammonium acetate, pH 9, in 5% ACN/95% water, and 100% ACN as buffer B. Detection was carried out in negative ion mode. The MS was calibrated using Low concentration Tune Mix (Agilent, Waldbronn, Germany). For confirmation of metabolite identity, high resolution extracted ion chromatograms of theoretical ion masses (+/- 0.005 Da) were generated in Bruker Data Analysis 4.1. If possible, additional MRM experiments were performed with an isolation width of 5 Da and collision energy of 30eV with nitrogen as collision gas was used. In all

experiments, three masses were fragmented in one method and the resulting mass spectra compared against reference spectra from the measured standards and the METLIN database.

2.5 Statistical analysis

Reproducibility of MSI data was evaluated by mean ± standard deviation.

3. RESULTS

3.1. MALDI-FTICR-MSI detection and localization of metabolites in the retina

Figure 1 is the workflow for the MALDI-FTICR-MSI of light- and dark-treated mammalian retina. Following light- or dark-treatment, retina samples are coated in 9-AA matrix. The matrix was deposited using a SunCollect sprayer, resulting in fine crystal size (~20 µm) and homogenous coverage (Figure 2A). Hierarchical clustering, in which similar spectra are grouped using multivariate statistical analysis, was conducted using the in-built FlexImaging 4.0 function, and used to generate segmentation maps (Figure 2B) [24, 25]. These segmentation maps are then used to identify areas in which similar spectra occur across the tissue sample (Figure 2C). Using this approach, MALDI-FTICR-MSI of our sample resolved more than 600 mass peaks with a single full MS scan.

From the 600 peaks, we identified 23 different metabolites belonging to a broad range of metabolic pathways using *in situ* MSI on the MALDI-FITCR. Figure 3 shows the distribution of the 23 metabolites across the retina. These were nucleotides AMP, ADP, ATP, UMP, UDP, UTP, GMP, GDP, GTP, IMP, and glucose-6-phosphate (G6P), fructose-1,6-bis-phosphate (F1,6bP), N-acetylaspartate (NAA), citrate and glycerol-mono-phosphate from the central carbon metabolism pathway. Additionally, we detected metabolites from a number of different pathways such as desulfoglucotropeolin from 2-oxocarboxylic acid metabolism, pyrophosphate from oxidative phosphorylation, sn-glycero-3-phosphoethanolamine from

glycerophospholipid metabolism, 3-sulfino-L-alanine and gluthathione from cysteine and methionine metabolism, and glycerophosphoinositol lipids.

The identities of AMP, ADP, ATP, UMP, UDP, UTP, GMP, GDP, GTP, IMP, G6P, F1,6bP, citrate, NAA, glycerol-mono-phosphate, and glutathione, were confirmed by comparison with LC-full mass scan data and/or MS/MS spectra of standard compounds (supplementary data 1). As MALDI-FTICR-MS has a high-resolving power (>100,000) and sub-ppm mass accuracy, it is capable of resolving metabolite peaks with similar nominal masses of compounds, metabolites and endogenous species in full scan mode often without the requirement for MS/MS [7, 26]. Therefore, desulfoglucotropeolin, pyrophosphate, sn-glycerol-3-phosphoethanolamine, 3-sulfino-L-alanine and glycerophosphoinositols were identified by matching accurate mass with databases (mass accuracy 2 ppm). These findings demonstrate the potential of MALDI-FTICR-MS for highly sensitive *in situ* metabolomics imaging, which can lead to an enhanced understanding of biological mechanisms.

3.2. In situ imaging of the central metabolism pathway in light- and dark- treated retina

The retina possesses many interesting metabolic properties, including high rates of oxygen consumption and varied electrical activity depending on glucose concentration [27-29]. We examined differences in the central metabolism pathway of dark and light-treated porcine retina. An overview and comparison of the metabolic profiles under these conditions is presented in Figure 4. Reproducibility of MSI data was evaluated by mean ± standard deviation (5 biological replications). All standard deviations were within 20% indicating similarity of individual measurement (supplementary data 2).

In dark-treated retinas, G6P (*m/z* 259.0220) from glycolysis and F1,6bP (*m/z* 338.9890) from the glycolysis and pentose phosphate pathway present similar localization profiles with both *m/z* values detected at high intensities in the outer and inner retina. Citrate (*m/z* 191.0200), from the TCA cycle, followed a similar pattern, localizing evenly across the entire retina. N-acetylaspartate (NAA, *m/z* 174.0410), which has a variety of proposed roles in the central nervous system [30], and lipid metabolism intermediate glycerol monophosphate (*m/z* 171.0065) were also detected evenly across the retina.

A number of notable differences were found in the distribution profiles of the detected metabolites between light- and dark-treated samples, particularly those from the glycolysis pathway. Under the light-treated samples, G6P was detected at high intensities in both the outer and inner retina, but F1,6bP has completely shifted to the inner retina. Detected in the outer retina in the dark-treated samples, NAA is almost completely localized to the inner retina following light treatment, and citrate decreased in the outer retina and increased in the inner retina following light exposure. Glycerol monophosphate distribution remained unchanged from dark-treated tissues.

4. DISCUSSION

To gain a better understanding of retinal metabolism, we conducted *in situ* metabolomic imaging using a highly sensitive MALDI-FTICR-MS system, and examined differences in the retina following light and dark treatment. Porcine retinas were used to investigate the spatial localization of metabolites linked to central metabolism pathway and how they are altered in two different sensory conditions.

4.1. High-resolution metabolite imaging

Mass spectrometry imaging techniques are emerging as a powerful tool for the analysis of molecular distributions in biological samples [5, 6]. Unlike traditional mass spectrometry, sample preparation methods do not result in the loss of spatial localization, while allowing non-targeted analysis. Compared with immunohistochemistry, this allows detection of many molecules simultaneously as well as discovery of novel markers. In particular, MALDI-TOF MSI is capable of discriminating proteins within a wide range of samples from whole animal sections or specific organs [31, 32], and investigating of specific questions such as tumor prognostic biomarker detection or discrimination between tumor types [33, 34]. While MALDI-TOF is a straightforward and a regularly used approach to MSI, the detection of molecules below *m/z* 1000 is complicated by ions from the matrix and compounds endogenous in the sample [35]. FTICR is capable of higher resolution and mass accuracy than other analyzers primarily due to the greater stability of a superconducting magnet compared to radio frequency voltage such as that found in an quadrupole ion trap [36]. The ability of MALDI-FTICR MSI to detect low molecular weight compounds has been demonstrated in studies examining olanzapine and imatinib in tissue samples and methamphetamine in a single hair sample [7, 8], while other groups have found that 9-AA matrix is suitable for investigating samples in low-mass ranges [37, 38]. The study presented here combines these two approaches to investigate metabolism within the mammalian retina. By combining MALDI-FTICR-MS with the use of 9-AA matrix, we were able to detect a broad range of metabolites from a number of different pathways, such as glycolysis and the TCA cycle, nucleotides, and lipids within the mammalian retina. A similar study had previously been conducted using 9-AA and mouse brain [37], and we were able to detect several of the same metabolites in retinal sections. More interestingly, we have demonstrated

that this approach is able to differentiate between different metabolic states of the same tissue.

4.2. MALDI-MSI of the retina

MALDI-MSI of the eye has been relatively limited, possibly due to difficulties in handling ocular tissues. MSI studies of the lens have examined the distributions of proteins such as aquaporin 0 [39], MP20 [39], Apolipoprotein E and collagen VI [40]. Additionally, a number of studies have examined distributions of crystallin proteins and peptides in the lens [41, 42], and their alterations in age and disease [43-45]. MALDI-MSI of the retina has primarily used MALDI-TOF-MS and concentrated on lipid distributions. These studies can also be divided into two main areas – studies that utilized whole preparations and those that use retinal sections. Studies of whole mouse and human retina have examined the distribution of *N*-retinylidene-*N*-retinylethanolamie (A2E) [46, 47], a major component of lipofuscin which has roles in aberrant cholesterol metabolism and is thought to play a role in the development of age-related macular degeneration [48]. Interestingly, these MALDI-MSI studies found contrasting distributions between the mouse and human samples with a correlation between A2E and lipofuscin fluorescence in mouse tissue that was not present in human retina. Using sectioned retinal tissue, MALDI-MSI studies have found that the distributions of different phospholipids and fatty acids follow the different retinal layers [49-51], while others have used this technique to examine drug penetration and metabolism within ocular tissues [52-54]. However, while the previous studies utilized MALDI-TOF-MS or nano-particle-assisted laser desorption/ionization, we believe our study to be the first to utilize MALDI-FTICR-MS to examine the central metabolism pathway (glycolysis, TCA) within the normal retina.

4.3. Metabolism within the outer retina.

Anatomically and functionally, the retina can be separated into two distinct sections: the outer retina which is populated with photoreceptors that transform light into electrical signals, and the inner retina containing signal-processing neurons. Many studies have been conducted comparing the effect of outer or inner retinal location and illumination on retinal metabolism, and for simplicity we will also examine our findings with respect to outer versus inner retina [10, 11, 13-15, 17, 55, 56].

In our study, MALDI-FTICR imaging of dark-treated retina detected G6P, F1,6bP, citrate, and NAA within the outer retina. With the exception of G6P, which is unchanged, all of these compounds were decreased in light-treated outer retina. The relatively higher amounts of all metabolites under dark conditions reflect the function of photoreceptors and their specialized metabolic requirements. Photoreceptors are known to be among the most metabolically demanding cells in the body as they are depolarized and constantly release the neurotransmitter glutamate in the dark, requiring constant Na^+/K^+-ATPase activity to maintain plasma membrane potential and Ca^{2+} flux for synaptic transmission [57]. Photoreceptors have a high density of mitochondrial and glycolytic proteins [58], as befitting their metabolically demanding status, which would account for our detection of these products in these cells. In response to light stimulation, photoreceptors hyperpolarize and cease neurotransmitter release, thereby decreasing their metabolic demands. Indeed, glycolysis and glucose oxidation within the outer retina has been measured as being 42% lower in light conditions than in the dark [10]. The relative stability of G6P levels in contrast to the other detected metabolites in the outer retina could therefore be due to a slowing of glycolytic activity. The outer retina is avascular and is nourished by the choroid. Choroidal blood flow is not altered by light stimulation [56], and so while the delivery rate of glucose

and glucose phosphorylation remains the same as in dark conditions, decreased glycolytic activity results in decreased levels of downstream metabolites such as F1,6bP following exposure to light.

4.4. Metabolism of the inner retina

Our MALDI-FTICR images of the inner retina indicate the presence of G6P, F1,6bP, citrate, NAA and glycerol monophosphate at similar levels in both dark and light-treated retina. Studies using different techniques have reported no difference in inner retinal metabolism between light and dark conditions [11, 17, 59, 60], although functional studies have indicated an increase in neuronal activity in light conditions [61, 62]. Shih and colleagues suggested that a possible reason for the lack of metabolic change in the inner retina between light and dark conditions is due to the responses of post-receptoral neurons in response light [56]. In the mammalian retina, the post-photoreceptor signaling can be split into two broad categories – the 'ON' and 'OFF' pathways, both of which are activated by photoreceptor activity. In the dark, photoreceptor glutamate release hyperpolarizes 'ON' bipolar cell and depolarizes 'OFF' bipolar cells. Light stimulation and photoreceptor hyperpolarization reverses this activity, resulting in 'ON' bipolar cell depolarization and 'OFF' bipolar cells hyperpolarization (for an overview of retinal function, see [12]). Shih and colleagues suggest that because the activity of ON and OFF bipolar cells is reversed in light from dark, as opposed to a complete change in activity such as seen in photoreceptors, the lack of net activity changes could account for why there is no measurable difference in metabolism [56]. Our findings of unchanged central metabolism pathways compound levels in dark and light-treated retina is therefore in agreement with previous reports.

4.5. Wider use of metabolite imaging

Our study has revealed the distribution of metabolites in the retina and demonstrated differences in biocompounds associated with the central metabolism pathway in the retina in light and dark conditions. It is important to understand these unique distributions as many diseases of the retina exhibit or are derived from metabolic disturbances [18, 63-65]. Diabetic retinopathy (DR) is a major complication of diabetes, which affects over 90% of type 1 and 60% of type 2 diabetics after two decades of disease [66]. A large number of biochemical alterations are known to occur within diabetic retina that affect metabolite levels, such as Na+/K+ATPase dysfunction [19], altered amino-acid neurotransmitter metabolism [67], and a decreased abundance of NADH dehydrogenase (ubiquinone) subunits[68]. As a phosphorylated form of glucose, the distribution of G6P and other glycolysis metabolites would be ideal metabolites to examine in DR. G6P dehydrogenase (G6PD) catalyzes the conversion of G6P to 6-phosphogluconolactone as the first step of the pentose phosphate pathway. G6PD deficiency has been linked with increased prevalence of type 2 diabetes [69], while type 1 (juvenile) diabetic patients with a G6PD deficiency have been found have an increased prevalence of proliferative retinal microvasculature complications [70]. Likewise, glycolysis is known to be altered in diabetic retina, although the exact nature of its dysfunction is matter of debate. One study using direct measurements of metabolites reported accumulated F1,6bP and therefore increased glycolysis [71], while another study using NMR spectroscopy indicated that glycolysis rates were decreased [72]. Additionally, as hyperglycaemia is known to affect the activity of a number of glycolysis-associated pathways, it would be useful to use MSI to determine how fluctuations in other metabolites, such as sorbitol from the polyol pathway, changes in diabetes.

5. CONCLUDING REMARKS

This highly sensitive MS imaging technique allowed the visualisation of the distributions of a broad range of metabolites simultaneously in mammalian retina. These findings highlight the potential applications of this *in situ* metabolomics imaging technique for the visualization of spatiotemporal dynamics of the tissue metabolome. MSI offers unique advantages over traditional mass spectrometry and autoradiography techniques in that the spatial distribution of varied classes of molecular species, including peptides, proteins, lipids, drugs and metabolites, can be determined using the same platform. Implementation of MSI qualitative and quantitative data for both endogenous and exogenous molecular species from different compound classes has widespread impact on clinical research and study of disease mechanisms. In this way, molecules can be interrogated in their native environments, providing new insights into the biological processes at systems biology level and facilitating understanding of disease processes and finding of novel biomarkers.

FUNDING SOURCES

The study was supported by Ministry of Education and Research of the Federal Republic of Germany (BMBF) (Grant Nos. SysTec-Verbund IMAGING FKZ 0315508A to MU and AW, 01IB10004E to AW) and the Deutsche Forschungsgemeinschaft (Grant Nos HO 1258/3-1, SFB 824 TP Z02 and WA 1656/3-1) to AW.

ACKNOWLEDGMENTS

Claudia-Marieke Pflüger, Mian Wei, Ulrike Buchholz, Gabriele Mettenleiter and Andreas Voss from the Research Unit Analytical Pathology, and Nicole Senninger from the Research Unit Protein Science provided technical assistance.

CONFLICT OF INTEREST STATEMENT

The authors have declared no conflict of interest.

SUPPORTING INFORMATION

The MS/MS and LC-MS data are provided in supplementary data 1. Reproducibility of metabolite MSI are represented in supplementary data 2.

REFERENCES

[1] Fiehn, O., Metabolomics--the link between genotypes and phenotypes. *Plant Mol Biol* 2002, *48*, 155-171.
[2] Miura, D., Fujimura, Y., Wariishi, H., In situ metabolomic mass spectrometry imaging: recent advances and difficulties. *J Proteomics* 2012, *75*, 5052-5060.
[3] Sugiura, Y., Honda, K., Kajimura, M., Suematsu, M., Visualization and quantification of cerebral metabolic fluxes of glucose in the awake mice. *Proteomics* 2013.
[4] Balluff, B., Rauser, S., Ebert, M. P., Siveke, J. T., *et al.*, Direct molecular tissue analysis by MALDI imaging mass spectrometry in the field of gastrointestinal disease. *Gastroenterology* 2012, *143*, 544-549 e541-542.
[5] Caprioli, R. M., Farmer, T. B., Gile, J., Molecular imaging of biological samples: localization of peptides and proteins using MALDI-TOF MS. *Anal Chem* 1997, *69*, 4751-4760.
[6] Pol, J., Strohalm, M., Havlicek, V., Volny, M., Molecular mass spectrometry imaging in biomedical and life science research. *Histochem Cell Biol* 2010, *134*, 423-443.
[7] Cornett, D. S., Frappier, S. L., Caprioli, R. M., MALDI-FTICR imaging mass spectrometry of drugs and metabolites in tissue. *Anal Chem* 2008, *80*, 5648-5653.
[8] Miki, A., Katagi, M., Kamata, T., Zaitsu, K., *et al.*, MALDI-TOF and MALDI-FTICR imaging mass spectrometry of methamphetamine incorporated into hair. *J Mass Spectrom* 2011, *46*, 411-416.
[9] Taban, I. M., Altelaar, A. F., van der Burgt, Y. E., McDonnell, L. A., *et al.*, Imaging of peptides in the rat brain using MALDI-FTICR mass spectrometry. *J Am Soc Mass Spectrom* 2007, *18*, 145-151.
[10] Wang, L., Tornquist, P., Bill, A., Glucose metabolism in pig outer retina in light and darkness. *Acta Physiol Scand* 1997, *160*, 75-81.
[11] Wang, L., Tornquist, P., Bill, A., Glucose metabolism of the inner retina in pigs in darkness and light. *Acta Physiol Scand* 1997, *160*, 71-74.
[12] Wässle, H., Parallel processing in the mammalian retina. *Nat Rev Neurosci* 2004, *5*, 747-757.
[13] Wang, L., Kondo, M., Bill, A., Glucose metabolism in cat outer retina. Effects of light and hyperoxia. *Invest Ophthalmol Vis Sci* 1997, *38*, 48-55.
[14] Okawa, H., Sampath, A. P., Laughlin, S. B., Fain, G. L., ATP consumption by mammalian rod photoreceptors in darkness and in light. *Curr Biol* 2008, *18*, 1917-1921.
[15] Linton, J. D., Holzhausen, L. C., Babai, N., Song, H., *et al.*, Flow of energy in the outer retina in darkness and in light. *Proc Natl Acad Sci U S A* 2010, *107*, 8599-8604.
[16] Hagins, W. A., Penn, R. D., Yoshikami, S., Dark current and photocurrent in retinal rods. *Biophys J* 1970, *10*, 380-412.
[17] Braun, R. D., Linsenmeier, R. A., Goldstick, T. K., Oxygen consumption in the inner and outer retina of the cat. *Invest Ophthalmol Vis Sci* 1995, *36*, 542-554.
[18] Wallace, D. C., Singh, G., Lott, M. T., Hodge, J. A., *et al.*, Mitochondrial DNA mutation associated with Leber's hereditary optic neuropathy. *Science* 1988, *242*, 1427-1430.
[19] Ottlecz, A., Garcia, C. A., Eichberg, J., Fox, D. A., Alterations in retinal Na+, K(+)-ATPase in diabetes: streptozotocin-induced and Zucker diabetic fatty rats. *Curr Eye Res* 1993, *12*, 1111-1121.
[20] Simo, R., Hernandez, C., Neurodegeneration is an early event in diabetic retinopathy: therapeutic implications. *Br J Ophthalmol* 2012, *96*, 1285-1290.
[21] Ting, A. Y., Lee, T. K., MacDonald, I. M., Genetics of age-related macular degeneration. *Curr Opin Ophthalmol* 2009, *20*, 369-376.

[22] Weymouth, A. E., Vingrys, A. J., Rodent electroretinography: methods for extraction and interpretation of rod and cone responses. *Prog Retin Eye Res* 2008, *27*, 1-44.
[23] Yuan, M., Breitkopf, S. B., Yang, X., Asara, J. M., A positive/negative ion-switching, targeted mass spectrometry-based metabolomics platform for bodily fluids, cells, and fresh and fixed tissue. *Nature protocols* 2012, *7*, 872-881.
[24] Alexandrov, T., Becker, M., Deininger, S. O., Ernst, G., *et al.*, Spatial segmentation of imaging mass spectrometry data with edge-preserving image denoising and clustering. *Journal of proteome research* 2010, *9*, 6535-6546.
[25] Alexandrov, T., Becker, M., Guntinas-Lichius, O., Ernst, G., von Eggeling, F., MALDI-imaging segmentation is a powerful tool for spatial functional proteomic analysis of human larynx carcinoma. *Journal of cancer research and clinical oncology* 2013, *139*, 85-95.
[26] Römpp, A., Guenther, S., Takats, Z., Spengler, B., Mass spectrometry imaging with high resolution in mass and space (HR(2) MSI) for reliable investigation of drug compound distributions on the cellular level. *Analytical and bioanalytical chemistry* 2011, *401*, 65-73.
[27] Ames, A., 3rd, Gurian, B. S., Effects of glucose and oxygen deprivation on function of isolated mammalian retina. *Journal of neurophysiology* 1963, *26*, 617-634.
[28] Winkler, B. S., The electroretinogram of the isolated rat retina. *Vision research* 1972, *12*, 1183-1198.
[29] Winkler, B. S., Glycolytic and oxidative metabolism in relation to retinal function. *The Journal of general physiology* 1981, *77*, 667-692.
[30] Moffett, J. R., Namboodiri, A. M., Preface: a brief review of N-acetylaspartate. *Adv Exp Med Biol* 2006, *576*, vii-xiii.
[31] Attia, A. S., Schroeder, K. A., Seeley, E. H., Wilson, K. J., *et al.*, Monitoring the inflammatory response to infection through the integration of MALDI IMS and MRI. *Cell Host Microbe* 2012, *11*, 664-673.
[32] Lagarrigue, M., Becker, M., Lavigne, R., Deininger, S. O., *et al.*, Revisiting rat spermatogenesis with MALDI imaging at 20-microm resolution. *Mol Cell Proteomics* 2011, *10*, M110 005991.
[33] Balluff, B., Rauser, S., Meding, S., Elsner, M., *et al.*, MALDI imaging identifies prognostic seven-protein signature of novel tissue markers in intestinal-type gastric cancer. *Am J Pathol* 2011, *179*, 2720-2729.
[34] Meding, S., Nitsche, U., Balluff, B., Elsner, M., *et al.*, Tumor classification of six common cancer types based on proteomic profiling by MALDI imaging. *J Proteome Res* 2012, *11*, 1996-2003.
[35] Krutchinsky, A. N., Chait, B. T., On the nature of the chemical noise in MALDI mass spectra. *J Am Soc Mass Spectrom* 2002, *13*, 129-134.
[36] Shi, S. D. H., Drader, J. J., Freitas, M. A., Hendrickson, C. L., Marshall, A. G., Comparison and interconversion of the two most common frequency-to-mass calibration functions for Fourier transform ion cyclotron resonance mass spectrometry. *International Journal of Mass Spectrometry* 2000, *195*, 591-598.
[37] Miura, D., Fujimura, Y., Tachibana, H., Wariishi, H., Highly sensitive matrix-assisted laser desorption ionization-mass spectrometry for high-throughput metabolic profiling. *Anal Chem* 2010, *82*, 498-504.
[38] Miura, D., Fujimura, Y., Yamato, M., Hyodo, F., *et al.*, Ultrahighly sensitive in situ metabolomic imaging for visualizing spatiotemporal metabolic behaviors. *Anal Chem* 2010, *82*, 9789-9796.
[39] Thibault, D. B., Gillam, C. J., Grey, A. C., Han, J., Schey, K. L., MALDI tissue profiling of integral membrane proteins from ocular tissues. *J Am Soc Mass Spectrom* 2008, *19*, 814-822.

[40] Ronci, M., Sharma, S., Chataway, T., Burdon, K. P., *et al.*, MALDI-MS-imaging of whole human lens capsule. *J Proteome Res* 2011, *10*, 3522-3529.
[41] Han, J., Schey, K. L., MALDI tissue imaging of ocular lens alpha-crystallin. *Invest Ophthalmol Vis Sci* 2006, *47*, 2990-2996.
[42] Grey, A. C., Schey, K. L., Distribution of bovine and rabbit lens alpha-crystallin products by MALDI imaging mass spectrometry. *Mol Vis* 2008, *14*, 171-179.
[43] Grey, A. C., Schey, K. L., Age-related changes in the spatial distribution of human lens alpha-crystallin products by MALDI imaging mass spectrometry. *Invest Ophthalmol Vis Sci* 2009, *50*, 4319-4329.
[44] Stella, D. R., Floyd, K. A., Grey, A. C., Renfrow, M. B., *et al.*, Tissue localization and solubilities of alphaA-crystallin and its numerous C-terminal truncation products in pre- and postcataractous ICR/f rat lenses. *Invest Ophthalmol Vis Sci* 2010, *51*, 5153-5161.
[45] Su, I. H., Basavaraj, A., Krutchinsky, A. N., Hobert, O., *et al.*, Ezh2 controls B cell development through histone H3 methylation and Igh rearrangement. *Nat Immunol* 2003, *4*, 124-131.
[46] Grey, A. C., Crouch, R. K., Koutalos, Y., Schey, K. L., Ablonczy, Z., Spatial localization of A2E in the retinal pigment epithelium. *Invest Ophthalmol Vis Sci* 2011, *52*, 3926-3933.
[47] Ablonczy, Z., Higbee, D., Anderson, D. M., Dahrouj, M., *et al.*, Lack of correlation between the spatial distribution of A2E and lipofuscin fluorescence in the human retinal pigment epithelium. *Invest Ophthalmol Vis Sci* 2013, *54*, 5535-5542.
[48] Lakkaraju, A., Finnemann, S. C., Rodriguez-Boulan, E., The lipofuscin fluorophore A2E perturbs cholesterol metabolism in retinal pigment epithelial cells. *Proc Natl Acad Sci U S A* 2007, *104*, 11026-11031.
[49] Hayasaka, T., Goto-Inoue, N., Sugiura, Y., Zaima, N., *et al.*, Matrix-assisted laser desorption/ionization quadrupole ion trap time-of-flight (MALDI-QIT-TOF)-based imaging mass spectrometry reveals a layered distribution of phospholipid molecular species in the mouse retina. *Rapid Commun Mass Spectrom* 2008, *22*, 3415-3426.
[50] Hayasaka, T., Goto-Inoue, N., Zaima, N., Shrivas, K., *et al.*, Imaging mass spectrometry with silver nanoparticles reveals the distribution of fatty acids in mouse retinal sections. *J Am Soc Mass Spectrom* 2010, *21*, 1446-1454.
[51] Roy, M. C., Nakanishi, H., Takahashi, K., Nakanishi, S., *et al.*, Salamander retina phospholipids and their localization by MALDI imaging mass spectrometry at cellular size resolution. *J Lipid Res* 2011, *52*, 463-470.
[52] Brignole-Baudouin, F., Desbenoit, N., Hamm, G., Liang, H., *et al.*, A new safety concern for glaucoma treatment demonstrated by mass spectrometry imaging of benzalkonium chloride distribution in the eye, an experimental study in rabbits. *PLoS One* 2012, *7*, e50180.
[53] Drexler, D. M., Tannehill-Gregg, S. H., Wang, L., Brock, B. J., Utility of quantitative whole-body autoradiography (QWBA) and imaging mass spectrometry (IMS) by matrix-assisted laser desorption/ionization (MALDI) in the assessment of ocular distribution of drugs. *J Pharmacol Toxicol Methods* 2011, *63*, 205-208.
[54] Yamada, Y., Hidefumi, K., Shion, H., Oshikata, M., Haramaki, Y., Distribution of chloroquine in ocular tissue of pigmented rat using matrix-assisted laser desorption/ionization imaging quadrupole time-of-flight tandem mass spectrometry. *Rapid Commun Mass Spectrom* 2011, *25*, 1600-1608.
[55] Bui, B. V., Kalloniatis, M., Vingrys, A. J., The contribution of glycolytic and oxidative pathways to retinal photoreceptor function. *Invest Ophthalmol Vis Sci* 2003, *44*, 2708-2715.

[56] Shih, Y. Y., Wang, L., De La Garza, B. H., Li, G., *et al.*, Quantitative retinal and choroidal blood flow during light, dark adaptation and flicker light stimulation in rats using fluorescent microspheres. *Curr Eye Res* 2013, *38*, 292-298.
[57] Wong-Riley, M. T., Energy metabolism of the visual system. *Eye Brain* 2010, *2*, 99-116.
[58] Reidel, B., Thompson, J. W., Farsiu, S., Moseley, M. A., *et al.*, Proteomic profiling of a layered tissue reveals unique glycolytic specializations of photoreceptor cells. *Mol Cell Proteomics* 2011, *10*, M110 002469.
[59] Lau, J. C., Linsenmeier, R. A., Oxygen consumption and distribution in the Long-Evans rat retina. *Exp Eye Res* 2012, *102*, 50-58.
[60] Medrano, C. J., Fox, D. A., Oxygen consumption in the rat outer and inner retina: light- and pharmacologically-induced inhibition. *Exp Eye Res* 1995, *61*, 273-284.
[61] De La Garza, B. H., Li, G., Shih, Y. Y., Duong, T. Q., Layer-specific manganese-enhanced MRI of the retina in light and dark adaptation. *Invest Ophthalmol Vis Sci* 2012, *53*, 4352-4358.
[62] Hoshi, H., Sato, M., Oguri, M., Ohtsuka, T., In vivo nitric oxide concentration in the vitreous of rat eye. *Neurosci Lett* 2003, *347*, 187-190.
[63] Yu, D. Y., Cringle, S. J., Retinal degeneration and local oxygen metabolism. *Exp Eye Res* 2005, *80*, 745-751.
[64] Junk, A. K., Goel, M., Mundorf, T., Rockwood, E. J., Bhattacharya, S. K., Decreased carbohydrate metabolism enzyme activities in the glaucomatous trabecular meshwork. *Mol Vis* 2010, *16*, 1286-1291.
[65] Lim, L. S., Mitchell, P., Seddon, J. M., Holz, F. G., Wong, T. Y., Age-related macular degeneration. *Lancet* 2012, *379*, 1728-1738.
[66] Fong, D. S., Aiello, L., Gardner, T. W., King, G. L., *et al.*, Diabetic retinopathy. *Diabetes Care* 2003, *26*, 226-229.
[67] Ishikawa, A., Ishiguro, S., Tamai, M., Changes in GABA metabolism in streptozotocin-induced diabetic rat retinas. *Curr Eye Res* 1996, *15*, 63-71.
[68] Ly, A., Scheerer, M. F., Zukunft, S., Muschet, C., *et al.*, Retinal Proteome Alterations in a Mouse Model of Type 2 Diabetes. *Diabetologia* 2013, *In press*.
[69] Heymann, A. D., Cohen, Y., Chodick, G., Glucose-6-phosphate dehydrogenase deficiency and type 2 diabetes. *Diabetes Care* 2012, *35*, e58.
[70] Cappai, G., Songini, M., Doria, A., Cavallerano, J. D., Lorenzi, M., Increased prevalence of proliferative retinopathy in patients with type 1 diabetes who are deficient in glucose-6-phosphate dehydrogenase. *Diabetologia* 2011, *54*, 1539-1542.
[71] Van den Enden, M. K., Nyengaard, J. R., Ostrow, E., Burgan, J. H., Williamson, J. R., Elevated glucose levels increase retinal glycolysis and sorbitol pathway metabolism. Implications for diabetic retinopathy. *Invest Ophthalmol Vis Sci* 1995, *36*, 1675-1685.
[72] Santiago, A. R., Garrido, M. J., Cristovao, A. J., Duarte, J. M., *et al.*, Evaluation of the impact of diabetes on retinal metabolites by NMR spectroscopy. *Curr Eye Res* 2010, *35*, 992-1001.

Figure 1: A workflow for the MALDI imaging of light- and dark-treated mammalian retina. Porcine eyes were used as the model systems. Light- and dark-treated retinas were transversely cryosectioned at 12 μm, coated with 9-AA matrix and analyzed with MALDI-FTICR-MS. By comparing the signal intensities of light and dark-treated retinas, metabolites with different expression profiles can be illustrated.

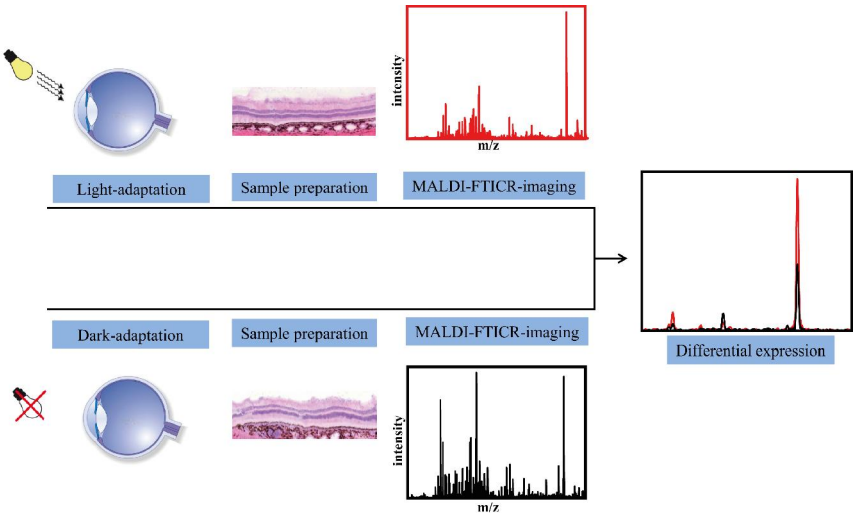

Figure 2: High spatial resolution-MSI allows resolving of the layered structure of the retina. A: A microscope image of 9-AA matrix crystals demonstrates homogenous coverage consisting of crystals approximately 20 µm in size. B: Hierarchical clustering based on multivariate statistical analysis of similar peak populations generates segmentation maps of the imaging data set. C: MSI images of different metabolites which are located on different retina layers. As examples, glutathione, fructose-1,6-bisphosphate and glucose-monophosphate are shown.

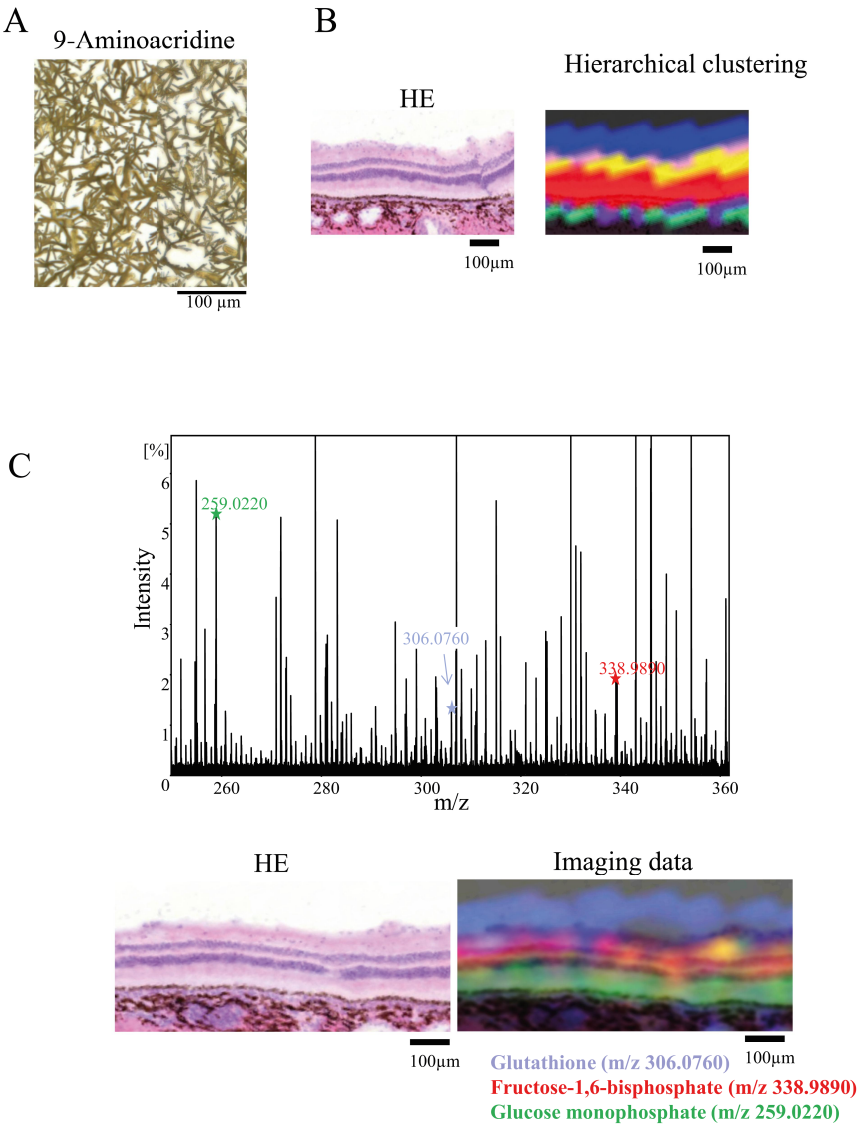

Figure 3. *In situ* MALDI-FTICR-MSI of dark-treated retina. MS imaging data were acquired in negative ion mode with 50 µm spatial resolution. A broad range of metabolites including nucleotides, central metabolism pathway, 2-oxocarboxylic acid metabolism, oxidative phosphorylation, glycerophospholipid metabolism, cysteine and methionine and lipids were simultaneously visualized in a single MS imaging experiment. The region of retina section shown above as stained with H&E shows the spatial distribution of the detected compounds (RPE, retinal pigment epithelium; OS, outer segment; IS, inner segment; ONL, outer nuclear layer; OPL, outer plexiform layer; INL, inner nuclear layer; IPL, inner plexiform layer; GCL, ganglion cell layer).

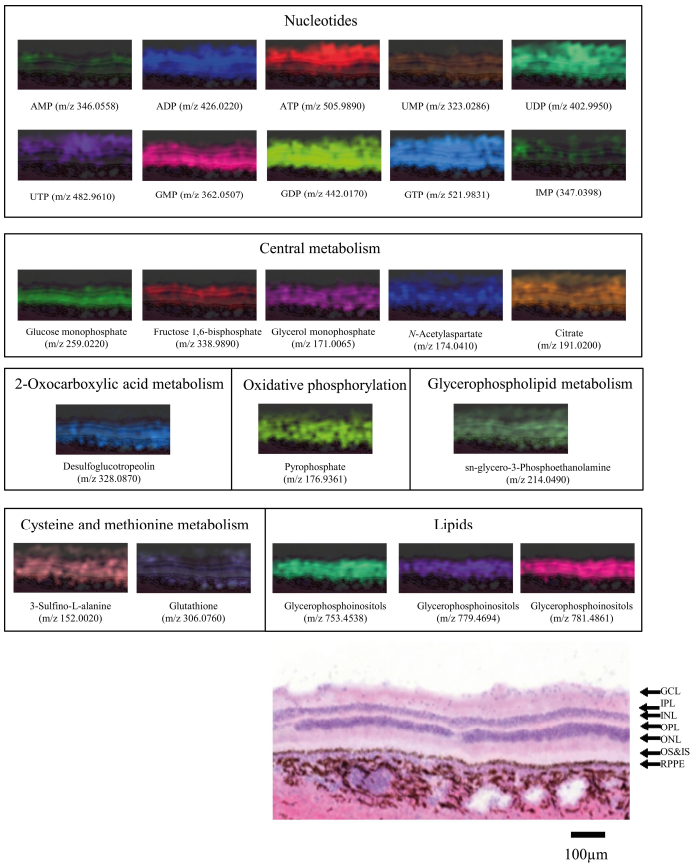

Figure 4: *In situ* central metabolism pathway imaging of retinas that had either been maintained in the dark or treated with light. Cryosectioned retina slices (12 µm thickness) were used for the *in situ* metabolite imaging. Mass-resolved imaging data were acquired in negative ion mode at 50 µm spatial resolution. All imaging data were normalized against the root mean square of all data points for quantitative comparison of the concentration of each metabolite under the different conditions. P = phosphate.

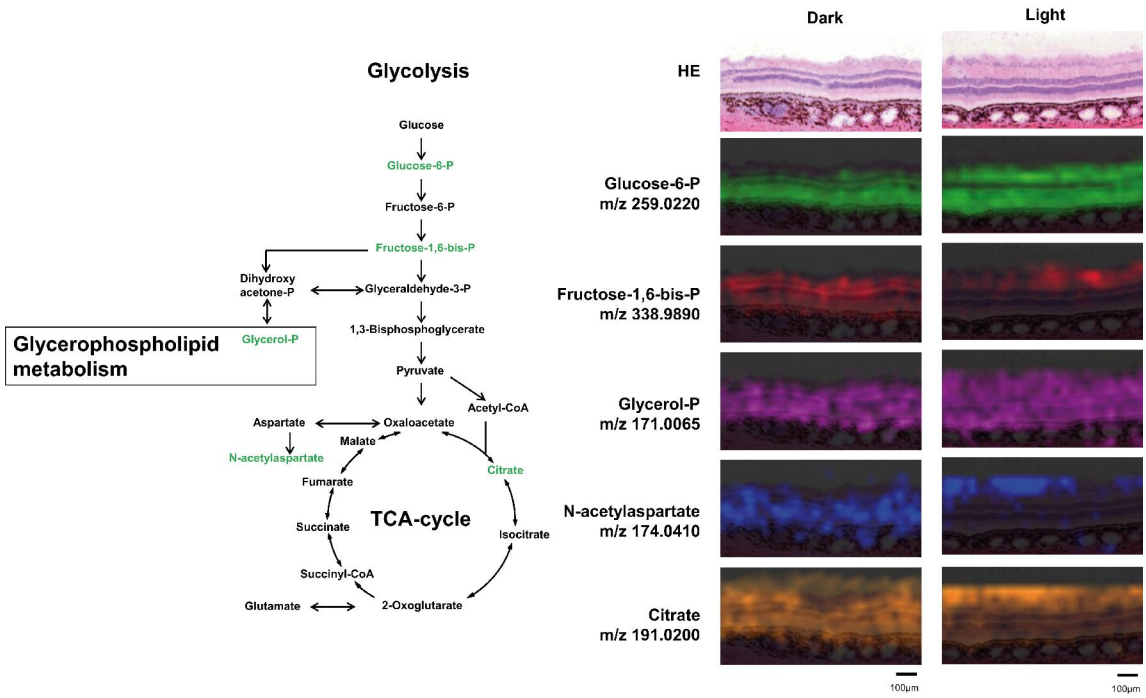

Table 1. List of chemical standards used for LC-MS/MS validation experiments.

Name	Sigma-Aldrich Catalogue number
AMP	A2252-5G
ADP	A2754-100MG
ATP	FLAAS-1VL
UMP	U6375-1G
UDP	94330-100MG
UTP	94370-250MG
GMP	G8377-500MG
GDP	G7127-25MG
GTP	G8877-25MG
IMP	I4625-5G
Glutathione	G4251-1G
Glucose monophosphate	G7250-500MG
Fructose 1,6-bisphosphate	F6803-1G
Glycerol monophosphate	94124-10MG
N-Acetylaspartate	00920-5G
Citrate	251275-5G